Article

Not peer-reviewed version

# Hydroxyapatite Modified Zeolite for Fluoride Removal in Drinking Water: Adsorption Mechanism Investigation and Column Study

Rajinda Boteju , Libing Zheng * , H. M. S. Wasana , Qiyang Wu , Yuansong Wei * , Hui Zhong , Yawei Wang , Ajith De Alwis

Posted Date: 28 February 2025

doi: 10.20944/preprints202502.2203.v1

Keywords: Fluoride; Adsorption; Zeolite; Hydroxyapatitie (HAp); Drinking water

 doi:10.20944/preprints202502.2203.v1



*Article*

# Hydroxyapatite Modified Zeolite for Fluoride Removal in Drinking Water: Adsorption Mechanism Investigation and Column Study

**Rajinda Boteju [1, 2,3], Libing Zheng [1,2,3,4*], H.M.S. Wasana [5], Qiyang Wu [1,2,3], Yuansong Wei [1,2,3, *], Hui Zhong[1,2], Wang Yawei[1,2] and Ajith de Alwis [6]**

[1] State Key Joint Laboratory of Environmental Simulation and Pollution Control, Research Center for Eco-Environmental Sciences, Chinese Academy of Sciences, Beijing 100085, China

[2] Laboratory of Water Pollution Control Technology, Research Center for Eco-Environmental Sciences, Chinese Academy of Sciences, Beijing 100085, China

[3] University of Chinese Academy of Sciences, Beijing 100049, China

[4] Department of Chemical Engineering, KU Leuven, 3001 Leuven, Belgium.

[5] Postgraduate Institute of Agriculture, University of Peradeniya, Peradeniya 20400, Sri Lanka

[6] Department of Chemical and Process Engineering, Faculty of Engineering, University of Moratuwa, Moratuwa 10400, Sri Lanka

* Correspondences: lbzheng@rcees.ac.cn (L.Z.); yswei@rcees.ac.cn (Y.W.); Tel.: +86-10-6284-9690 (Y.W.)

**Abstract:** This study investigates the synthesis and application of Hydroxyapatite (HAp)-modified zeolite materials for efficient fluoride removal from groundwater-based drinking water. The characterization confirmed the successful incorporation of HAp onto the zeolite surface and the formation of a stable composite. EDS analysis revealed the presence of Ca and P after modification, while FTIR and XRD confirmed the structural integrity of HAp during adsorption. The ZH8 exhibited the highest F- removal efficiency of 92.23% at pH 3. Meanwhile, the HAp-modified zeolite showed high F- selectivity, the competing ions, like chloride and bromide, had limited interference. Isotherm studies revealed that the Langmuir model best described the adsorption process, suggesting monolayer adsorption with a maximum capacity of 39.38 mg/g for ZH8. Kinetic studies indicated that the process followed pseudo-first-order kinetics, with equilibrium achieved within 4 hours. Regeneration studies demonstrated that ZH8 maintained over 85% efficiency for three cycles, highlighting its reusability. Column studies validated the material's practical applicability, with breakthrough times of up to 23 hours under optimal conditions (flow rate: 8 $cm^3$ $min^{-1}$, bed depth: 30 cm, feed concentration: 7.5 ppm). Thomas model best described the column adsorption process, indicating chemical adsorption as the dominant mechanism. These findings demonstrate the potential of HAp-modified zeolite, particularly ZH8, as an effective adsorbent for fluoride removal in real-world applications.

**Keywords:** Fluoride; Adsorption; Zeolite; Hydroxyapatitie (HAp); Drinking water

## 1. Introduction

The presence of fluoride in drinking water has become a growing concern due to its potential adverse effects on human health. Numerous studies have highlighted the detrimental effects of long-term consumption of drinking water with a high fluoride concentration [1–5]. Dental and skeletal fluorosis are among the most commonly observed health issues associated with excessive fluoride intake through drinking water. To ensure the safety and well-being of individuals, the removal of fluoride from potable water is paramount. Fluoride levels in the North-Central Province in Sri Lanka are significantly higher than the permissible limit, especially during the dry season, and more than 1/3 of the ground water sources are exceeding the permissible limit (1.0 mg/L) [6]. Additionally,

 doi:10.20944/preprints202502.2203.v1



recent studies suggest a synergistic effect between fluoride, cadmium, and water hardness in contributing to chronic kidney disease of unknown etiology (CKDu) in Sri Lanka [7]. Moreover, small-scale drinking water treatment plants in rural Sri Lanka, particularly those using Reverse Osmosis (RO) as the primary membrane process, face challenges in consistently delivering safe drinking water due to seasonal variations, especially in the North, North-Central, and North-Western provinces. These variations affect water quality, making it difficult to maintain acceptable standards [8].

There are several methods for removing fluoride from drinking water sources such as coagulation and precipitation, electro-coagulation (EC), ion exchange, dialysis, electro-dialysis and membrane processes [9]. Coagulation and precipitation involve aggregating particles [10]. However, this method is costly, produce harmful sludge, and depend on interfering ions. EC uses electric charge to initiate coagulation with efficiency influenced by factors like pH, current density etc. [11]. The high initial cost and operational cost and amount of sludge handling caused this method non cost effective [12]. Ion exchange involves swapping fluoride ions with other ions like chloride onto a resin. This is a physical separation process which depends on the resin's functional groups [13]. The preparation of specific resin is costly [12], and the regeneration process is not sustainable [9]. Despite being energy-efficient, dialysis is limited to industrial usage due to slow kinetics [9]. Electro-dialysis (ED) uses electric current and ion-selective membrane [14]. Although, the high energy consumption and the capital investment are the main challenges for ED operations [15]. Nanofiltration (NF) and reverse osmosis (RO) are prominent membrane methods, with NF being more cost-effective than RO due to lower pressure and energy requirements [9]. However, hazardous concentrate handling, expensive capital investment and extensive operational costs make membrane processes a challenging task.

Among the various technologies available for fluoride removal in drinking water, adsorption has emerged as one of the most effective and widely used methods due to its cost-effectiveness, ease of operation and simple design [16–18]. Several adsorbents for adsorption have been investigated in past decades for their potential to remove fluoride from drinking water and those can be categorized as, carbon-based materials, metal-based materials, polymers and resins, metal organic frameworks (MOFs), bio materials and natural materials. Among these materials, natural materials have gained considerable attention as promising adsorbents for fluoride removal from water in recent years. Natural minerals, formed through geological processes, are cost-effective and environmentally friendly materials widely used for fluoride removal due to their unique properties, such as high surface area, ion exchange capacity, and chemical stability molecular sieve structure, and diverse surface and structural properties [19]. Moreover, the materials prepared with clay-based minerals showed comparable or even better fluoride separation capacity than other available options [20]. These materials consist of a combination of two or more components at the nanoscale level, resulting in unique properties and improved performance compared to individual component alone. In most of those materials, zeolite, montmorillonite, kaolinite and bentonite are used as the host material whereas rare earth metals like lanthanum, high affinity substances like aluminium, iron, zerconium, Hydroxyapatite are used for the surface modifications. Particularly, zeolite, an alumino-silicate material, is known for their excellent ion exchange and adsorption properties [18]. Surface modification of zeolites with organic and inorganic materials was performed to improve their anion adsorption capacity, addressing their inherent negative surface charge.[21–23].

The recent studies show that these surface modifications of zeolite materials are capable of removing Fluoride from water sources to mitigate the fluoride contamination. One of the latest studies, Zhao et al. investigated the removal of phosphate and fluoride using lanthanum hydroxide modified zeolite (LMZ) [24]. Results showed that LMZ effectively adsorbed both phosphate and fluoride, though fluoride adsorption capacity decreased by 57.9% in the presence of phosphate, which was unaffected. Another study also has used lanthanum-modified zeolites (LMZ), synthesized from coal fly ash, for efficient fluoride removal from water [25]. The maximum adsorption capacity was 141.5 mg/g at a F/La molar ratio of 4.21. Lanthanum modified zeolite was also used in another

 doi:10.20944/preprints202502.2203.v1



study done by Lai et al., which investigated the mechanism of fluoride removal from simulated zinc sulfate solutions [26]. The results demonstrated a maximum adsorption capacity of 20.83 mg/g at 303 K and 23.04 mg/g at 313 K. A composite adsorbent has synthesized using zirconium oxychloride, chitosan, and artificial zeolite for the removal of fluoride ($F^-$) from water in a study done by Chen et al. [27]. The adsorption isotherms fit the Freundlich and Langmuir models, with a maximum adsorption capacity of 10.75 mg/g at room temperature, suggesting chemisorption as the primary mechanism.

Coal fly ash was used in another study to synthesize aluminum hydroxide-coated zeolite (AHZ), which studied the efficient fluoride removal from wastewater [28]. The study demonstrated that AHZ has a maximum fluoride adsorption capacity of 18.12 mg/g. Over 92% of fluoride was removed within 2 hours. On another study done by Ebsa, explored defluoridation from drinking water using clinoptilolite zeolite modified with a cationic surfactant, hexadecy trimethyl ammonium bromide (HTAB) [29]. At a constant fluoride concentration of 10 mg/L and 5 g/L HTAB dosage, the highest fluoride removal efficiencies were achieved after 60 minutes. The study found that unmodified zeolite was ineffective for fluoride adsorption, while surfactant-modified zeolite required careful control of pH, temperature, and runtime. In a study done by Gao et al., micron zirconia/zeolite molecular sieve ($ZrO_2$-Ze) composite were synthesized to study the effect of fluoride removal in drinking water [30]. Optimal adsorption conditions were determined as an adsorbent dose of 2 g/150 mL, contact time of 8 hours, pH 6, and temperature of 25°C, achieving a fluoride removal rate of 94.89%. Natural zeolite was modified with magnesium (II), aluminum (III), and titanium (IV) ions, in a study done by Ma et al., as adsorbents for fluoride removal from wastewater [31]. The competitive adsorption tests demonstrated that the modified zeolites exhibited high selectivity for fluoride ions.

But in most of these studies, rare earth minerals are used and energy intensive modification routes are followed which are not cost-effective solutions. Among the high affinity substances, hydroxyapatite showed enhanced, efficient removal performances of fluoride in aqueous solutions in various studies done in recent years [32–35]. Hence, zeolite-based, Hydroxyapatite modified adsorbent has a potential to be introduced as an innovative solution for existing problems in water treatment plants in Sri Lanka. Therefore, in this study, a surface modification is achieved by simply precipitation of hydroxyapatite (HAp) onto synthetic zeolite beads. It was then characterized by various characterization techniques to ensure the successful incorporation of HAp onto the surface. Then the performance was evaluated by investigating the effect of pH and competing ions on removal efficiency of fluoride. After that the adsorption mechanism is studied by isotherm and kinetic experiments. Finally, the practical applicability was assessed by column study varying the main parameters like flow rate, feed concentration and bed height. The results of this work showed potential for F- removal and offered an idea for a safe drinking water supply.

## 2. Materials and Methods

### *2.1. Materials*

Raw zeolite beads with particle size of 5 mm were purchased from MACKLIN (Shandong Keyuan Biochemical Co., Ltd., China.). DI water was used for all the experiments. The reagents used in this study including $NaH_2PO_4$, NaOH, $CaCl_2$, $FeCl_3.6H_2O$ and HCl were all analytical grade.

### *2.2. Surface modification of raw zeolite*

The surface modification of zeolite with hydroxyapatite (HAp) was done by simple precipitation method which was used in a previous literature [32]. Firstly, a 400 ml of 0.0072 mol HAp precipitate solution was prepared in a conical flask. $NaH_2PO_4.2H_2O$ and NaOH was added followed by adding of $CaCl_2$. A precipitate is formed and the pH is adjusted according to the experimental procedure. Zeolites were dried in an oven at $150^0$C to open the pore channel on the surface before adding as pre-preparation. 10 g of zeolites beads were then added to the solution with constant stirring at $25^0$C. Then the solution was agitated at 120 rpm for 4 h at $35^0$C, after that the solution was aged at $25^0$C for

 doi:10.20944/preprints202502.2203.v1



12 h. Then the zeolite beads were filtered and washed with DI water until neutral pH is achieved were dried overnight at 75$^0$C. Finally, the prepared zeolite beads were kept in airtight containers for future use. The prepared materials were categorized according to the pH (6, 7, 8, 9, 10) of the HAp solution in which the Zeolite beads are added. Thus, the materials were named as ZH6, ZH7, ZH8, ZH9 and ZH10. The raw zeolite beads was named as Raw-Z.

*2.3. Characterization*

X-ray Diffraction spectra of the synthesized materials were obtained from D8 advance powder x-ray diffractometer (Bruker AXS, Germany) to analyze the crystalline structure. Material identification was done from XRD patterns using MDI Jade 6 software (MDI Materials Data Inc., USA). The elemental analysis was done by energy dispersive x-ray spectroscopy (Quattro C, Thermo Fisher Scientific Inc., USA). The materials were then further analyzed to investigate the bonding formation using fourier-tansform infrared spectroscopy (FTIR, Nicolet iZ10 FTIR spectrometer, Thermo Fisher Scientific Inc., USA). FTIR patterns were identified using OMNIC 8.2.0.387 software (Thermo Fisher Scientific Inc., USA).

*2.4. Batch Study*

Unless or otherwise stated all the batch experiments were carried out using a 6 ppm fluoride solution, 10 g/L adsorbent dose at 30$^0$C. As per the recent studies the maximum Fluoride level was 6.89 ppm with an average of 1.23 ppm and a standard deviation (STD) of 0.99 [6] in ground water in north-central province in Sri Lanka. Hence 6 ppm was chosen as the standard for batch studies which was prepared using 100 ppm Fluoride stock solution. The fluoride removal efficiency of each material was tested in pH 3, 4, 5, 6, 7, 8, 9 using a 50 ml of the fluoride solution. The pH is adjusted by using 1M NaOH and 1M HCl solutions and measured by laboratory pH meter (FP20, Mettler-Toledo GmbH, Switzerland). After adding the sorbent, the solution was kept in an incubator shaker for 6 h at 120 rpm. The shaker time period and the adsorbent dosage were determined by choosing the optimum results of the preliminary experiments. The final $F^-$ concentration is then measured using the $F^-$ ion specific electrode (PXSJ-216F ion meter, Shanghai Yidian Scientific Instrument Co. Ltd., China) by adding appropriate amount of total ionic strength adjustment buffer solution (TISAB). Experiment for each material was triplicated and the removal efficiency was calculated according to eq. 1:

$$R\% = \frac{C_o - C_e}{C_o} \times 100\% \quad (1)$$

where R% is the removal efficiency, $C_0$ is the initial concentration (mg/L) and $C_e$ is the equilibrium concentration (mg/L).

The effect of competing ions was tested using different cations ($Na^+$: 200 ppm, $K^+$: 25 ppm) and anions ($Cl^-$: 250 ppm, $Br^-$: 220 ppm, $NO_2^-$: 50 ppm, $NO_3^-$: 20 ppm, $SO_4^{2-}$: 280 ppm). The selection of these ions and its initial concentrations were based on the latest results obtained by previous investigation on the ground water quality in north-central province of Sri Lanka [7]. The experiment was done using a 400 ml volume of the fluoride solution at initial pH of 6. After adding the sorbent material, the solution was constantly stirred at 120 rpm for 6 h. 10 ml samples were then collected from 0 to 240 mins at 30 mins intervals. The samples were then analyzed for final concentrations of the ions by inductively coupled plasma optical emission spectrophotometer (Optima 8300, Perkin Elmer, USA) and ion chromatography (ICS-1000, CA, USA). After these studies it was seen that out of the five materials synthesized, ZH7 and ZH8 have the better performance for Fluoride removal. Thus, those materials were selected for the isotherm and kinetic study.

*2.5. Isotherm Study*

The concentrations of $F^-$ were varied from 0 to 400 ppm to study the effect of concentration on adsorption. In each 50 ml solution the initial pH was 6 and the interaction time was 6 h. After the

 doi:10.20944/preprints202502.2203.v1



equilibrium phase achieved the final concentration in the solution was measured and the amount of fluoride adsorbed ($q_e$, mg/g) was calculated by eq. 2:

$$q_e = \frac{C_0 - C_e}{C_s} \quad (2)$$

where $C_0$ is the initial concentration (mg/L), $C_e$ is the equilibrium concentration(mg/L) and $C_s$ is the adsorbent dosage (mg/L). The variation of $q_e$ with $C_e$ was then non-linearly fitted using three adsorption isotherm models: Langmuir, Freundlich and Temkin. The relevant equations for these models are given in section S1 (supplementary information).

*2.6. Kinetic Study*

The reaction kinetics were investigated by maintaining the same laboratory conditions during the kinetic study as in isotherm study. Samples were drawn from the solution initially at 5, 10, 15, 20, 30 mins and in 30 mins intervals afterwards up to 6 h duration to measure the concentration. The experiments were duplicated during the study and the amount of fluoride adsorbed at time t ($q_t$, mg/g) was calculated by eq. 3:

$$q_t = \frac{C_0 - C_t}{C_s} \quad (3)$$

where, $C_0$ is the initial concentration (mg/L), $C_t$ is the concentration at time t (mg/L) and $C_s$ is the adsorbent dosage (mg/L). The variation of $q_t$ with $C_e$ was then non-linearly fitted using three adsorption kinetic models: Pseudo-First Order, Pseudo-Second Order and Elovich. The relevant equations for these models are given in section S2 (supplementary information).

*2.7. Column Study*

Practical application of the synthesized material as a pre-treatment unit was investigated by a continuous flow fixed-bed column study. Three main experimental parameters – feed concentration, flow rate and bed depth – were selected which were used in other similar studies [32,36,37]. The range of fluoride was varied as 5, 7.5 and 10 ppm, flow rate as 8, 12, 16 $cm^3\ min^{-1}$ and bed depth as 20, 30, 50 cm. All the column runs were performed at $30^0$C and ambient pressure. For the complete utilization of the material bed, the contaminated water was fed from the bottom to top using a peristaltic pump. Samples were collected at 1 h intervals and the concentration was measured. The breakthrough point ($t_b$) was defined as the time at which the outlet concentration reaches the maximum permissible limit for fluoride in drinking water in Sri Lankan standard (1 ppm). The experimental values were further analyzed using three adsorption models: Thomas, Yoon-Nelson, Bohart-Adams. The details of these models are presented in section S3 (Supplementary information). To investigate the removal efficiency from t=0 up to $t_b$, breakthrough volume ($V_b$) and percentage yield ($Y_b$ %) were calculated as per equations 3-7:

$$m_{in,t_b} = \int_0^{t_b} C_0\, Q\ dt \quad (3)$$

$$m_{out,t_b} = \int_0^{t_b} C_t\, Q\ dt \quad (4)$$

$$m_{ads,t_b} = m_{in,t_b} - m_{out,t_b} \quad (5)$$

$$V_b = Q \times t_b \quad (6)$$

$$Y_b(\%) = \frac{m_{ads,t_b}}{m_{in,t_b}} \times 100\% \quad (7)$$

where, $t_b$ is the breakthrough time (h), $C_o$ is the feed concentration (mg $dm^{-3}$), $C_t$ is concentration at time t (mg $dm^{-3}$), Q is flow rate ($cm^3\ min^{-1}$), $m_{in,tb}$ is total mass of fluoride fed up to $t_b$, $m_{out,tb}$ is total

 doi:10.20944/preprints202502.2203.v1



mass of fluoride out up to $t_b$, $m_{ads,tb}$ is total mass of fluoride adsorbed up to $t_b$, $V_b$ is the breakthrough volume (L), $Y_b$ (%) is the percentage yield up to $t_b$.

## 3. Results and Discussion

### *3.1. Characterization of the modified zeolite*

#### 3.1.1. EDS

The EDS spectrum and elemental mapping in Figure 1a shows the elemental analysis of the zeolite material commercially purchased. According to the spectra, the high intensities at 1.4867, 1.7399 and 5.249 keV values indicate the elemental composition of Al, Si and O, respectively which are the main elements of the zeolite material. Other than that, an additional peak is observed at 1.0409 keV which corresponds to Na. It can be seen from the mapping that these elements are uniformly distributed along the surface of the material. Fig. 1b shows the EDS spectrum for the material after adsorption. All the five different materials synthesized (ZH6, ZH7, ZH8, ZH9, ZH10) showed the same EDS spectra and elemental mapping. After the surface modification, corresponding two peaks for element Ca and one peak for P are found in 0.341, 3.69 and 2.01 keV values which is a clear indication of successful incorporation of those elements to surface during the chemical precipitation process of HAp [$Ca_{10}(PO_4)_6(OH)_2$]. Also, the peak values and the distribution of those elements is consistent according to the spectra. The corresponding peak at 676.8 keV in Figure 1c after adsorption, confirms the favourable Fluoride uptake by the active adsorption sites during the adsorption process.

 doi:10.20944/preprints202502.2203.v1



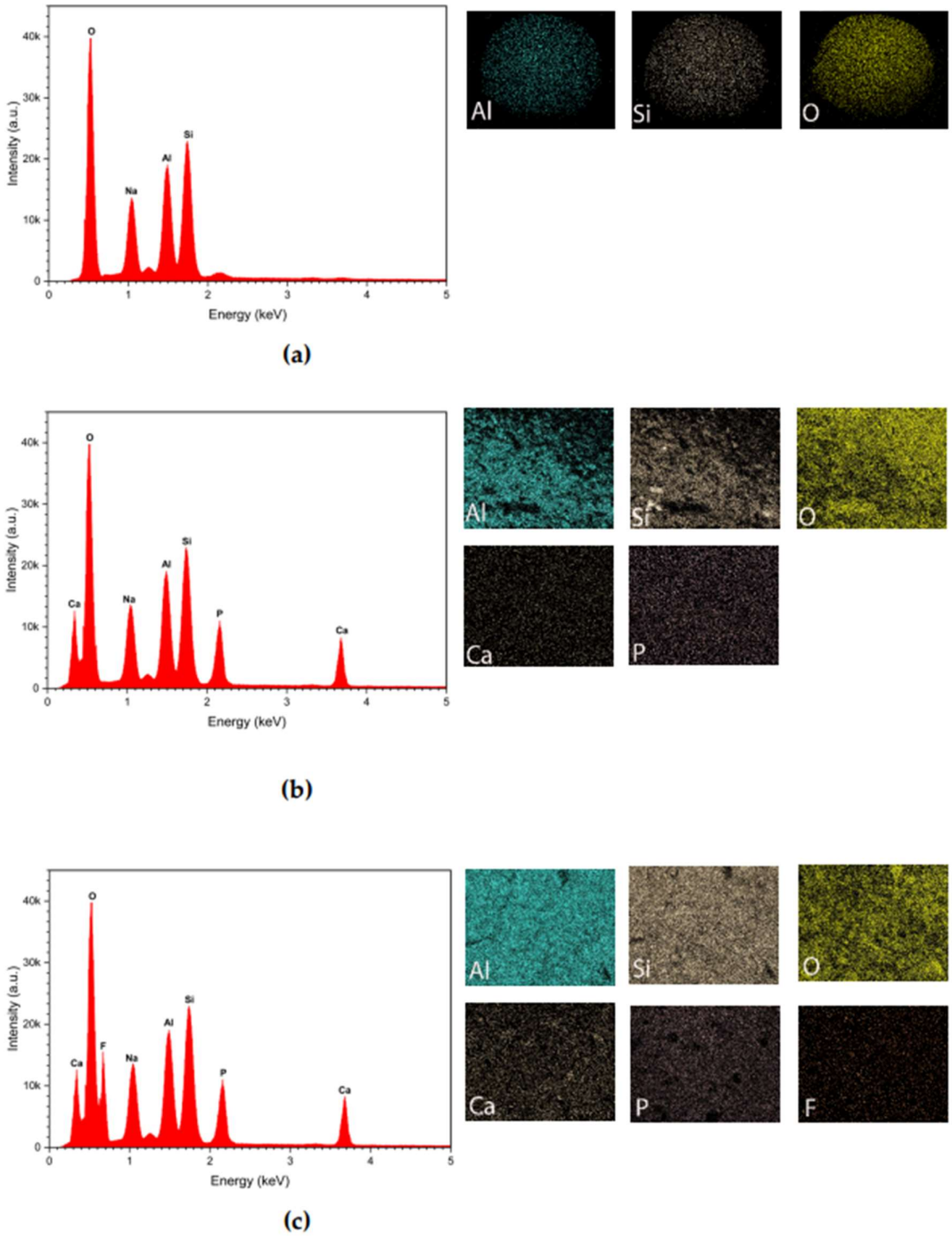


**Figure 1.** EDS spectra and elemental mapping of **(a)** Zeolite; **(b)** Zeolite after modification; **(c)** Zeolite after adsorption

3.1.2 FTIR

In order to study the functional groups in the synthesized materials, FTIR spectra were used and the results are illustrated Figure 2 and Figure S1. A broad peak in the range of 3685 – 3028 $cm^{-1}$ was discovered corresponding to stretching vibration of O-H group in raw Zeolite-A and another broad peak at 1651 $cm^{-1}$ was also discovered corresponding to bending vibration of the same ([38,39]). Also, the Si-O or Al-O asymmetric stretching modes were also detected at 1002 $cm^{-1}$. After modification a sharp peak was obtained at 1035 $cm^{-1}$ corresponding to stretching vibration of Phosphate ($PO_4^{3-}$) groups which is an indication of proper precipitation of HAp on to the surface of the material. A

 doi:10.20944/preprints202502.2203.v1



small peak was observed after adsorption at 756 $cm^{-1}$ which is corresponding to the formation of hydroxyl bonding of fluorohydroxyapatite [32]. That may be an indication of the adsorption process which might be described as a ligand exchange reaction [39]. Adsorption process didn't alter the bonding of Phosphate group which can be attributed as satisfactory formation good stability with the raw material.

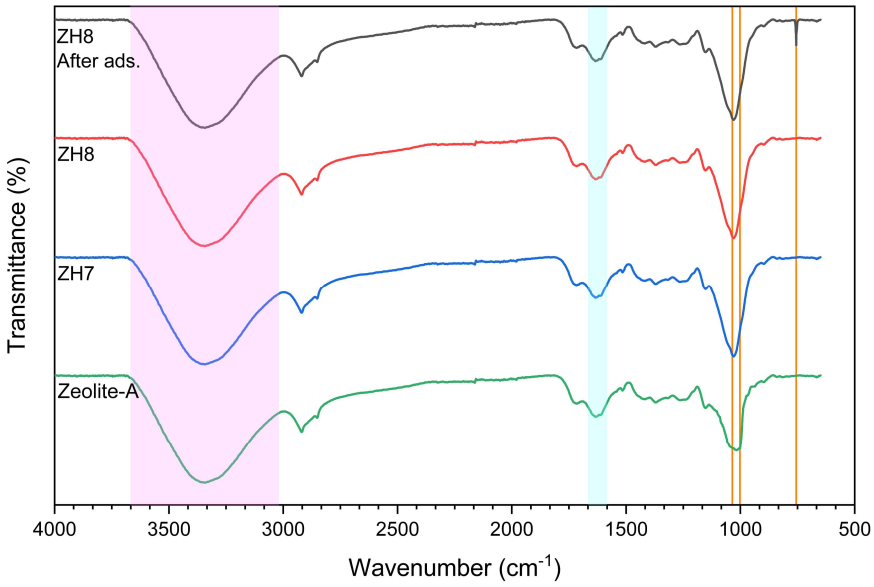


**Figure 2.** FTIR spectra of raw zeolite-A material, ZH7, ZH8 and ZH8 after adsorption

3.1.3 XRD

The X-ray diffraction (XRD) patterns for the synthetic zeolite and its surface-modified forms, ZH (zeolite modified with Hydroxyapatite) and ZH-8 after adsorption (ZH-8 After ads.), are presented in Figure 3 and patterns for other materials are presented Figure S2. The patterns reveal the crystalline nature of the zeolite, with its characteristic peaks prominently displayed at specific 2θ values. The peaks at 7.33°, 10.326°, 12.63°, 16.29°, 21.87°, 24.2°, 27.34°, 30.18°, and 34.43° can be attributed to the crystalline structure of the zeolite framework, consistent with previously reported literature for similar types of synthetic zeolites (ZeoliteA-syn, JCPDS 82-2400). These diffraction peaks are indicative of the well-ordered crystalline structure inherent to synthetic zeolite, corresponding to its microporous framework.

Following surface modification of the zeolite with Hydroxyapatite (HAp), the XRD pattern for ZH shows additional peaks at 31.9° and 49.8°, which are characteristic of HAp, indicating successful incorporation of the hydroxyapatite phase onto the zeolite surface (JCPDS 25-0166). The presence of these peaks suggests the formation of a composite material, where HAp is deposited on the zeolite surface, thereby enhancing the material's functionality for potential applications such of adsorption. Interestingly, the ZH modified samples showed a similar pattern to ZH, suggesting that substitution of HAp didn't make any changes in crystal structure of Zeolite-A. Since the Fluoride ions are replaced -OH groups in HAp, the crystal structure after adsorption is unaltered hence the XRD patterns remained identical. This result signifies the good stability of the synthesized adsorbents after adsorption [32].

 doi:10.20944/preprints202502.2203.v1



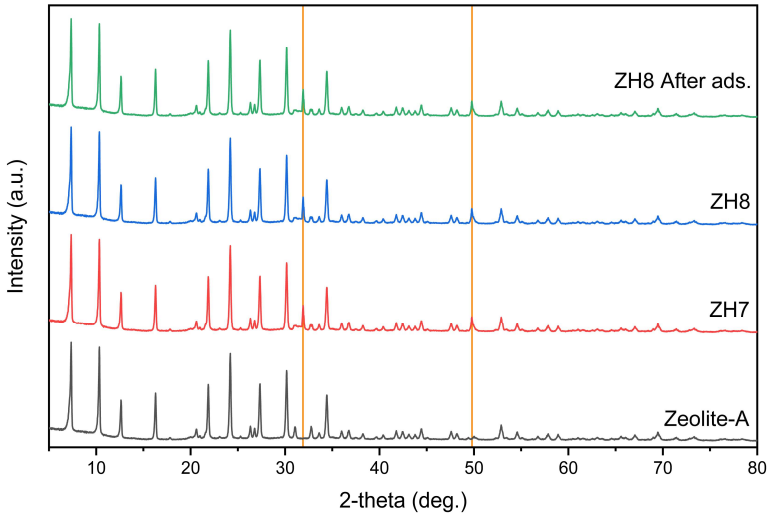


**Figure 3.** XRD spectra of raw zeolite-A material, ZH7, ZH8 and ZH8 after adsorption

*3.2 Adsorption performance*

3.2.1 Effect of pH on removal efficiency

Figure 4 illustrates the effect of pH on the removal efficiency (R%) of fluoride from water using five different materials synthesized, which showed a general trend of decreasing efficiency with increasing pH across all materials. The removal efficiency of the raw material was significantly enhanced by the incorporation of hydroxyapatite. The pH range was selected from 3 to 9, covering both acidic and basic conditions beyond the range of permissible pH for drinking water. At a low pH of 3, the removal efficiency is observed to be highest for all materials. ZH8 exhibited the highest efficiency of 92.23% while ZH9 showed the lowest efficiency at this pH. This trend indicates that fluoride removal is more effective under acidic conditions, which can be ascribed to increased protonation of active sites at lower pH, leading to stronger attraction of the negatively charged fluoride ions [39,40]. Removal efficiency of ZH8 remains somewhat stable during the drinking water pH range around the value of 67%.

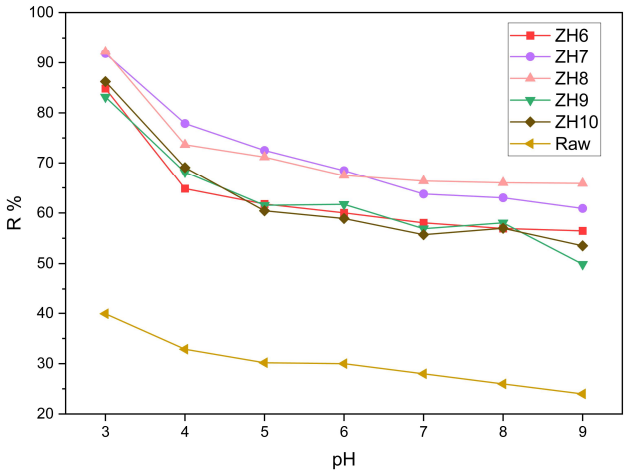


**Figure 4.** Effect on the removal efficiency at initial $F^-$ of 3 ppm

 doi:10.20944/preprints202502.2203.v1



3.2.2. Effect of competing ions

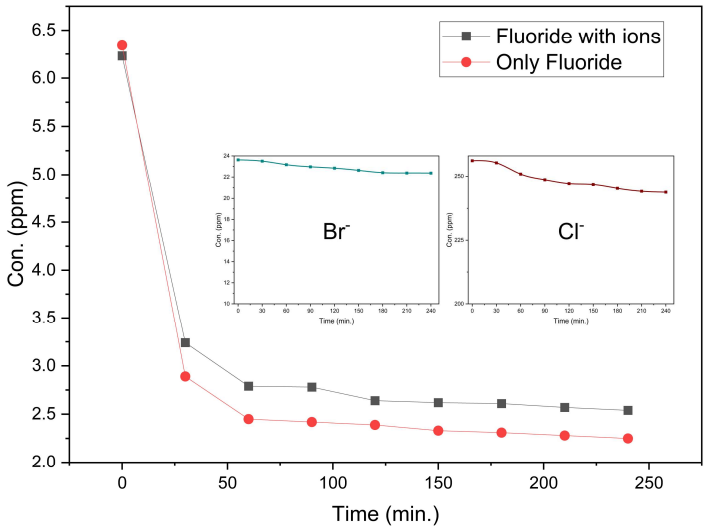


**Figure 5.** Variation of fluoride, bromide and chloride concentrations during the adsorption study for competing ions with ZH8

When the adsorption process happens in natural water sources, the adsorption surface not only attracts the fluoride ions but also the co-existing anions and cations. Thus, there may be a competition to fluoride ions for sorption on to the surface by some of those ions. Figure 5 shows the variation of concentration of fluoride, chloride and bromide ions during the adsorption process. As can be seen, the final concentration of Fluoride was higher than that of in the previous experiments, where the concentration of Chloride ions is also reduced with time. This can be correlated to the fact that Chloride has the same electronegativity, the valence as in fluoride ions and relatively lower ionic radius compared to other ions, hence interfered to the adsorption process. The concentrations of other ions remained constant during the whole time as seen from Figure S3. This result is an indication that the material ZH8 has a sorption selectivity for Fluoride and the coexisting ions have a limited interference in adsorption process.

*3.3 Adsorption mechanism*

3.3.1 Isotherm study

The Figure 6 shows the relationship between the equilibrium concentration of the adsorbate ($C_e$) and the amount adsorbed per unit mass of adsorbent ($q_e$). The Langmuir isotherm model, depicted by the red solid line, demonstrates a strong fit with the experimental data, for both materials implying adsorbent-adsorbate formed a monolayer and uniform active site with similar sorption energy [32,40]. The maximum adsorption capacity ($Q_m$) was determined to be 34.68 mg/g with a langmuir constant ($K_L$) of 0.807 L/mg for ZH7 and 39.38 mg/g with a langmuir constant ($K_L$) of 0.692 L/mg for ZH8. Adsorption intensity values (n) in Freundlich model for both the materials are greater than 1, which implies the favorable adsorption process for Fluoride removal [39]. In the Temkin isotherm model, heat of sorption ($B_T$) in Temkin Model for both materials which are 6.909 and 6.805 J/mg for ZH7 and ZH8 respectively, are positive indicating an exothermic reaction and since the value is greater than 0.385 J/mg, the adsorption is occurred as Chemisorption [41,42]. The relevant parameters for the models are provided in Table S1, although all models provided a good fit, the Langmuir model is superior, highlighting the homogeneity of the adsorption sites and the monolayer adsorption

 doi:10.20944/preprints202502.2203.v1



process as the dominant mechanism in this system. Amongst the two materials, ZH8 showed better adsorption performance.

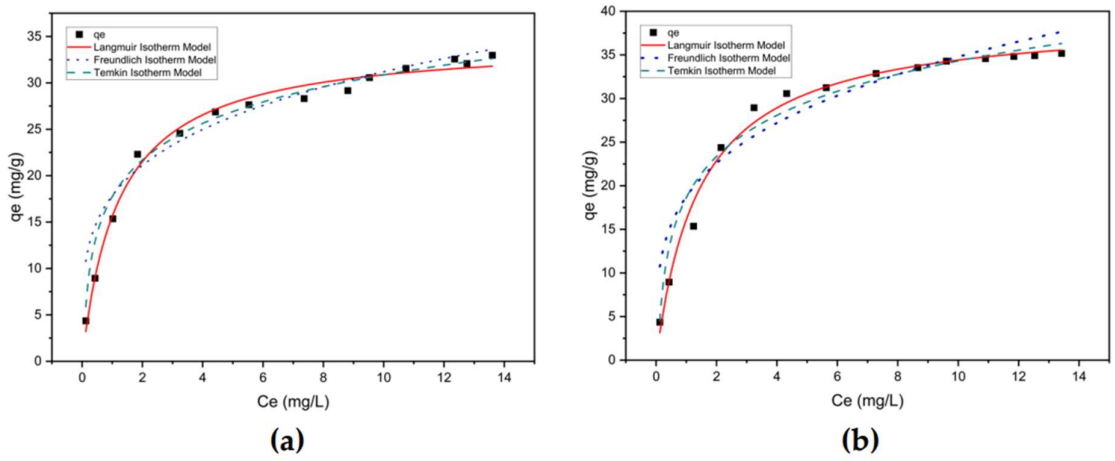


**Figure 6.** Adsorption isotherms of **(a)** ZH7 and **(b)** ZH8 (pH = 6, T = 303 K, Interaction time = 6 h, Dosage = 10 g/L)

3.3.2 Kinetic study

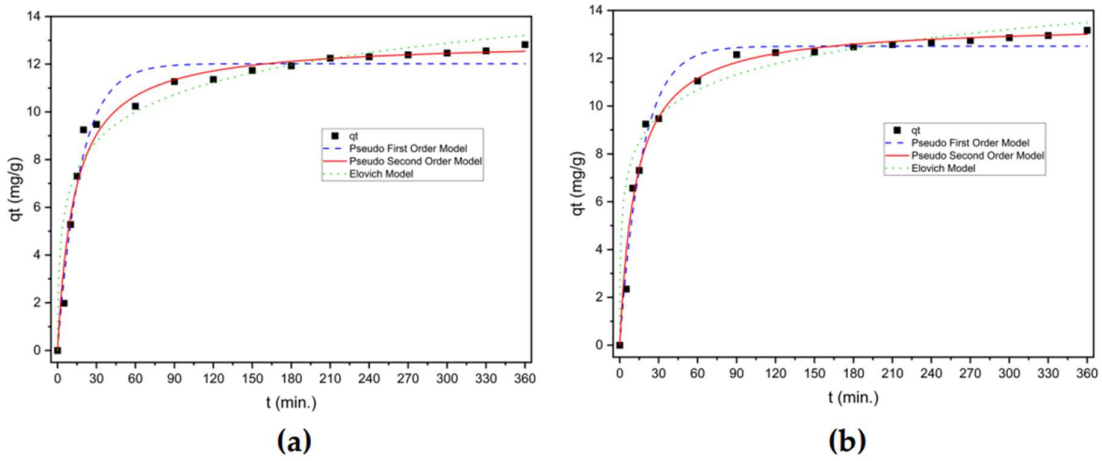


**Figure 7.** Adsorption kinetics of **(a)** ZH7 **(b)** ZH8 (Initial [$F^-$]= 6 ppm, pH = 6, T = 303 K, dosage = 10 g/L)

Fluoride ion removal ability was studied by the batch kinetic study of the two materials and the results are depicted in Figure 7. The contact time was kept up to 6 h. During the first 15 mins., the adsorption rate was rapid, due to the abundance of active sites on the surface, where more than 50% of the equilibrium adsorption capacity was achieved, which then was gradually risen during the next 210 mins. During this slow phase from 15 mins to 210 mins, the adsorption rate become sluggish due to the occupation of numerous energy sites resulting reduction in vacant active sites [39]. The equilibrium phase was achieved after 4 h in where the concentration remained almost unchanged. The fitting results are depicted in Table S2 for both the materials, analysis best fitted with Pseudo-first order model indicating the involvement of Chemical Adsorption [39,43]. Among the two materials, ZH8 showed the higher adsorption rate, implying it has more active sites and relatively higher potential surface area. Also, it has the higher correlation coefficient value from which it can be concluded that it is the best material in terms of adsorption kinetics.

 doi:10.20944/preprints202502.2203.v1



*3.4 Practical application study*

3.4.1 Regeneration and re-use

The results of regeneration and re-use study are illustrated in Figure 8. During the first three cycles the efficiency remained above 85% suggesting proper desorption of Fluoride and replacement of the -OH functional groups in HAp [32]. In 4$^{th}$ and the 5$^{th}$ cycles the efficiency is reduced below 80%. This can be attribute to the fact that there may be irrevocable active adsorption sites which couldn't replace the fluoride ions by -OH groups. However, still the efficiency is comparatively high up to 5 cycles. This suggest that the synthesized material, has a potential practical applicability for use for commercial purposes.

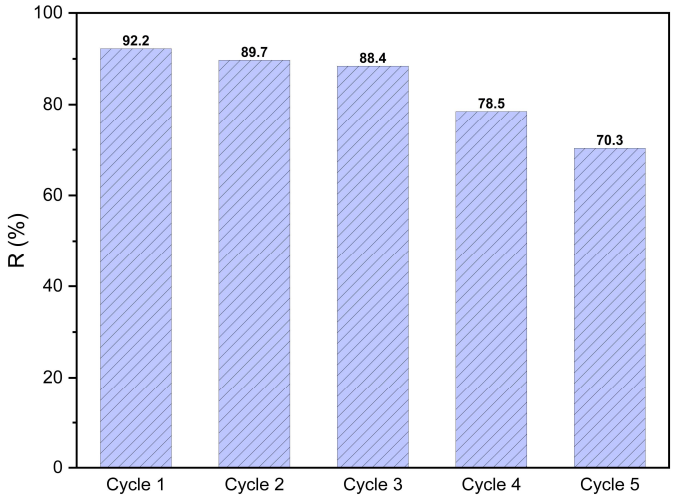


**Figure 8.** Regeneration study of ZH8 material

3.4.2 Column study

The breakthrough curve in figure 9a, displays the effects of varying flow rates on contaminant breakthrough time. The breakthrough times for flow rates of 8, 12, 16 cm3 min-1 were 23, 10.5, 4.5 h respectively. The trends indicated that, at increased flow rates, breakthrough occurred earlier, with a steeper curve slope, suggesting a shorter contact time between the material and the contaminated water. Further, when the flow is accelerated, it caused reduced residence time and insufficient time to achieve the equilibrium, limiting the efficiency of the adsorption process [36]. But at lower flow rates breakthrough times increased, producing a more gradual curve. That pattern can be attributed to the fact that, lower flow extended residence times within the column, allowing more time for adsorption interactions, hence providing sufficient time to reach the equilibrium [32]. Thus, optimizing flow rate would be essential for balancing throughput with contaminant removal efficiency. Slower flow rates may be beneficial for scenarios demanding high contaminant removal, while faster rates might suit for cases where higher processing volumes are needed for water with lower contaminant levels.

The impact of varying bed depths on the breakthrough time is revealed in figure 9b. The breakthrough times were observed to be 4.5, 10.5 and 16.5 h for bed depths of 20, 30 and 50 cm. Higher bed depths yield a more gradual breakthrough curve, indicating extended contaminant retention and prolonged saturation time compared to shorter bed depths, where breakthrough is faster, and the curve is steeper. Increased bed depth enhanced adsorption efficiency by providing a greater volume of adsorbent, thus increasing the number of active adsorption sites available for interaction with contaminants [32]. Moreover, greater bed depth provided a larger adsorption interface, delaying

 doi:10.20944/preprints202502.2203.v1



contaminant saturation and increasing the adsorption capacity. These results suggest that using deeper beds could reduce the frequency of adsorbent replacement or regeneration, ultimately leading to more suitable for real field applications.

The breakthrough curves for the effect of Feed concentration are presented in figure 9c. The Breakthrough times were 15, 10.5, 6.5 h for feed concentrations of 5, 7.5 and 10 ppm respectively. The breakthrough curve for higher concentrations is steeper compared to those for lower concentrations, providing that saturation is reached more quickly when the adsorbent is exposed to higher contaminant levels. This finding highlight that the adsorption active sites on the column's adsorbent material are occupied more quickly, leading to earlier breakthrough. This can be explained by the higher driving force resulted by higher concentration levels which leads to reduced breakthrough time. Also, when the concentration is high more Fluoride ions are introduced to the surface of the material per unit time inside the column which accelerates adsorption process hence saturation occurred more quickly than in lower concentration levels [36].

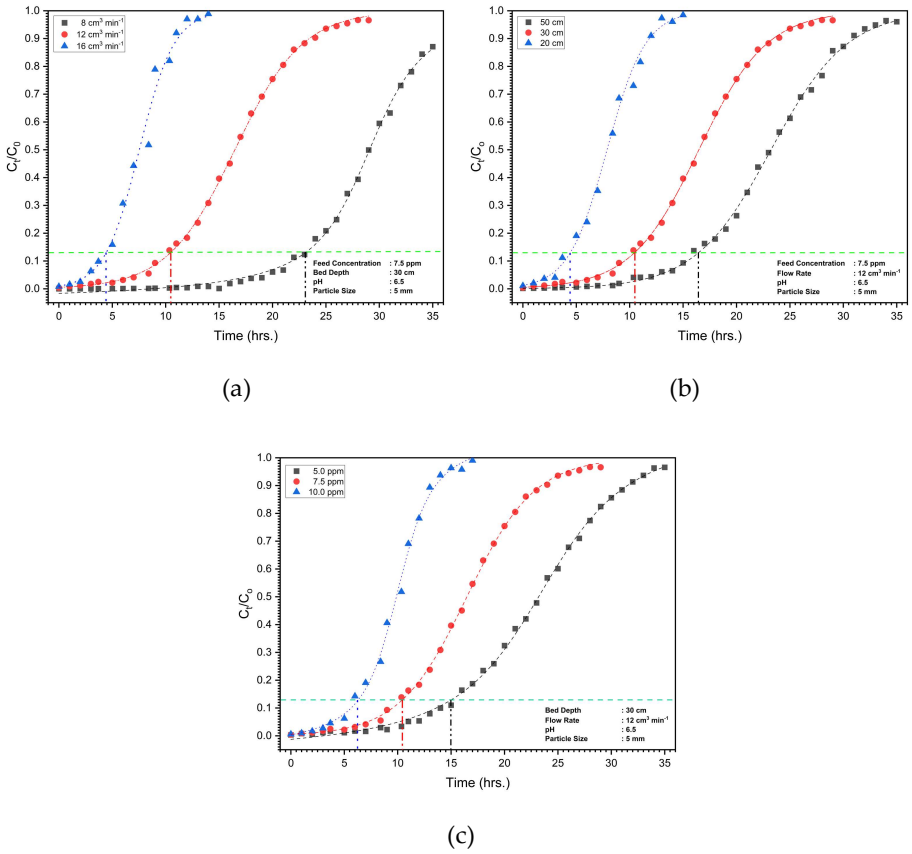


**Figure 9.** Breakthrough curves for fixed-bed adsorption columns; **(a)** Effect of flow rate, **(b)** Effect of bed depth, **(c)** Effect of feed concentration

The experimental parameter values for three adsorption models are presented in Table 1. The highest correlation coefficient ($R^2$) was reported for Thomas model which was greater than 0.995. This indicate that the adsorption process obeys Langmuir adsorption kinetics which matches the previously done isotherm studies. Moreover, according to the other assumptions in which the Thomas model was developed, plug flow occurs in the bed with no axial dispersion and the rate of adsorption is determined by chemical effects rather than diffusion [37]. The relationship between $k_{TH}$ and $q_0$ was inversely proportional and the highest uptake capacity of 6.96 mg $g^{-1}$ was reported when the bed depth was at maximum. The rate constant $k_{BA}$ and $N_0$ values in Bohart-Adams model was also inversely proportional which suggests the adsorption process is controlled by the external mass transfer over the initial phase of adsorption [36].

 doi:10.20944/preprints202502.2203.v1



**Table 1.** Mathematical parameters of Thomas, Yoon-Nelson and Bohart-Adams models

| Parameter | Thomas Model | | | Yoon-Nelson Model | | | Bohart-Adams Model | | |
|---|---|---|---|---|---|---|---|---|---|
| | $k_{TH}$ | $q_0$ | $R^2$ | $k_{YN}$ | $\tau$ | $R^2$ | $k_{BA}$ | $N_0$ | $R^2$ |
| **Bed Depth (cm)** | | | | | | | | | |
| 20 | 0.074 | 0.94 | 0.998 | 0.539 | 7.98 | 0.995 | 0.029 | 198.7 | 0.985 |
| 30 | 0.042 | 3.29 | 0.999 | 0.316 | 16.48 | 0.995 | 0.042 | 185.4 | 0.989 |
| 50 | 0.037 | 6.96 | 0.996 | 0.280 | 23.22 | 0.995 | 0.061 | 138.6 | 0.985 |
| **Flow Rate ($cm^3\ min^{-1}$)** | | | | | | | | | |
| 8 | 0.020 | 5.84 | 0.998 | 0.230 | 24.81 | 0.988 | 0.055 | 124.5 | 0.985 |
| 12 | 0.042 | 3.29 | 0.999 | 0.316 | 16.48 | 0.999 | 0.042 | 185.4 | 0.988 |
| 16 | 0.081 | 1.00 | 0.988 | 0.613 | 7.53 | 0.988 | 0.032 | 218.2 | 0.985 |
| **Feed Concentration ($mg\ dm^{-3}$)** | | | | | | | | | |
| 5 | 0.031 | 6.43 | 0.998 | 0.250 | 23.0 | 0.998 | 0.025 | 218.6 | 0.985 |
| 7.5 | 0.042 | 3.29 | 0.999 | 0.316 | 16.48 | 0.998 | 0.042 | 185.4 | 0.989 |
| 10 | 0.051 | 1.32 | 0.995 | 0.572 | 9.799 | 0.995 | 0.057 | 146.9 | 0.995 |

The results of the breakthrough volume ($V_b$) and percentage yield ($Y_b$%) are presented in the table 2. Since the best suited model was thomas model, that equation with the relevant $k_{TH}$ and $q_0$ parameter values for each experimental condition was used for $C_t/C_0$ term in the equation to calculate $m_{ads,tb}$. The yield exceeded 94% in five experimental conditions out of seven conditions. The yield was as high as 99% and 95% when the feed concentrations are 5 and 7 ppm which shows greater performance even at maximum polluted groundwater levels in Sri Lanka. From these results of the column study, it shows a potential of the materials ZH8 for Fluoride removal in groundwater in practical applications.

**Table 2.** Parameters related to removal efficiency of Fluoride up to breakthrough time ($t_b$)

| | Variation with Bed Depth (cm) | | | Variation with Flow Rate ($cm^3\ min^{-1}$) | | | Variation with Feed Concentration (ppm) | | |
|---|---|---|---|---|---|---|---|---|---|
| | 20 | 30 | 50 | 8 | 12 | 16 | 5 | 7.5 | 10 |
| $t_b$ | 4.5 | 10.5 | 16.5 | 23 | 10.5 | 4.5 | 15 | 10.5 | 6.5 |
| $m_{in,t_b}$ | 24.3 | 56.7 | 89.1 | 82.8 | 56.7 | 32.4 | 54 | 56.7 | 35.1 |
| $m_{ads,t_b}$ | 23.02 | 54.37 | 86.4 | 64.99 | 54.37 | 30.81 | 53.87 | 54.37 | 23.65 |
| $V_b$ | 3.24 | 7.56 | 11.88 | 11.04 | 7.56 | 4.32 | 10.80 | 7.56 | 4.68 |
| $Y_b$(%) | 94.73 | 95.88 | 96.94 | 78.48 | 95.88 | 95.1 | 99.77 | 95.88 | 67.37 |

## 5. Conclusions

In this study, a successful incorporation of hydroxyapatite (HAP) was done on to the surface of commercially available Zeolite beads (5 mm). The FTIR and XRD spectra indicates that the HAp structure of on the surface of the material wasn't altered during the adsorption process which indicated good stability with the raw material. Removal efficiency of ZH8 remains somewhat stable during the drinking water pH range around the value of 67%. The co-existing ions had a limited interference during the adsorption which showed the sorption selectivity for Fluoride of the material ZH8. The Langmuir model was best fitted ($R^2 > 0.98$) and maximum adsorption capacity ($Q_m$) was

 doi:10.20944/preprints202502.2203.v1



determined to be 34.68 mg/g with a Langmuir constant ($K_L$) of 0.807 L/mg for ZH7 and 39.38 mg/g with a Langmuir constant ($K_L$) of 0.692 L/mg for ZH8. Both ZH7 and ZH8 materials fitted with Pseudo-First Order model in the kinetic study which further indicated the involvement of chemical adsorption. Out of the five cycles run during the re-use, the efficiency remained above 85% during the first three cycles suggesting proper desorption of Fluoride and replacement of the -OH functional groups in HAp. Out of the three breakthrough models, thomas model was best fitted which obeys Langmuir adsorption kinetics and greater $R^2$ value (> 0.99) indicated the rate of adsorption is determined by chemical effects rather than diffusion. The highest yield was observed as 99% at feed concentration of 5 ppm and breakthrough volume was 10.8 liters which indicates a potential for practical application even at high fluoride contamination levels. In conclusion, the surface modified ZH8 material might be used as a solution for the existing fluoride contamination problems in groundwater of rural areas in Sri Lanka, in by using it as an adsorption pre-treatment column, for the existing membrane treatment train.

**Supplementary Materials:** The following supporting information can be downloaded at the website of this paper posted on Preprints.org. Section S1: Adsorption isotherms; Section S2: Adsorption kinetic models; Section S3: Breakthrough curve models; Figure S1: FTIR spectra of ZH6, ZH9 and ZH10; Figure S2: XRD spectra of ZH6, ZH9 and ZH10; Figure S3: Variation of a) Sodium b) Potassium c) Organic materials d) Nitrite e) Nitrate and f) Sulphate with time during the Fluoride adsorption process; Table S1: Modelling parameters of Isotherm study of ZH7 and ZH8 materials; Table S2: Modelling parameters of Kinetic study of ZH7 and ZH8 materials; Table S3: Experimental parameters of the column study.

**Author Contributions:** Conceptualization, Y.W., H.M.S.W., W. Y. and A. A.; Review and supervision, L.Z., Y.W. and H.M.S.W.; methodology, R.B. and Q.W.; software and analysis, R.B.; investigation, R.B.; Writing—original draft preparation and editing, R.B.; funding acquisition, Y.W. and H.Z., project administration, H.Z. All authors have read and agreed to the published version of the manuscript.

**Funding:** This research was funded by the International Scientists Project of Beijing Natural Science Foundation (IS24058), the Alliance of International Science Organizations Strategic Consulting Project (ANSO-SBA-2023-01), the Programme of the Comprehensive Studies on Sri Lanka (059GJHZ2023104MI), the Alliance of International Science Organization (ANSO) Scholarship for Young Talents (MSc: 2022ANSOM070), China-Sri Lanka Joint Research and Demonstration Center for Water Technology; China-Sri Lanka Joint Center for Education and Research, CAS.

**Data Availability Statement:** Data will be made available on request.

**Conflicts of Interest:** The authors declare no conflicts of interest

## References

1. Dar, F.A.; Kurella, S. Fluoride in Drinking Water: An in-Depth Analysis of Its Prevalence, Health Effects, Advances in Detection and Treatment. *Mater Today Proc* 2024, doi:10.1016/j.matpr.2023.05.645.
2. Ahmad, S.; Singh, R.; Arfin, T.; Neeti, K. Fluoride Contamination, Consequences and Removal Techniques in Water: A Review. *Environmental Science: Advances* 2022, *1*, 620–661.
3. Din, I.U.; Ali, W.; Muhammad, S.; Shaik, M.R.; Shaik, B.; Rehman, I. ur; Tokatli, C. Spatial Distribution and Potential Health Risk Assessment for Fluoride and Nitrate via Water Consumption in Pakistan. *J Geochem Explor* 2024, *259*, doi:10.1016/j.gexplo.2024.107413.
4. Huang, S.; Guo, J.; Xie, Y.; Bian, R.; Wang, N.; Qi, W.; Liu, H. Distribution, Sources, and Potential Health Risks of Fluoride, Total Iodine, and Nitrate in Rural Drinking Water Sources of North and East China. *Science of the Total Environment* 2023, *898*, doi:10.1016/j.scitotenv.2023.165561.
5. Tashauoei, H.R.; Mahdavi, M.; Mahvi, A.H.; Fatehizadeh, A. Dataset of Fluoride Concentration and Health Risk Assessment in Drinking Water in the Saveh City of Markazi Province, Iran. *Data Brief* 2023, *50*, doi:10.1016/j.dib.2023.109466.

6. Indika, S.; Hu, D.; Wei, Y.; Yapabandara, I.; Cooray, T.; Makehelwala, M.; Jinadasa, K.B.S.N.; Weragoda, S.K.; Weerasooriya, R.; Pang, Z. Spatiotemporal Variation of Groundwater Quality in North Central Province, Sri Lanka. *ACS ES and T Water* 2023, *3*, 1687–1698, doi:10.1021/acsestwater.2c00490.
7. Wasana, H.M.S.; Aluthpatabendi, D.; Kularatne, W.M.T.D.; Wijekoon, P.; Weerasooriya, R.; Bandara, J. Drinking Water Quality and Chronic Kidney Disease of Unknown Etiology (CKDu): Synergic Effects of Fluoride, Cadmium and Hardness of Water. *Environ Geochem Health* 2016, *38*, 157–168, doi:10.1007/s10653-015-9699-7.
8. Imbulana, S.; Oguma, K.; Takizawa, S. Evaluation of Groundwater Quality and Reverse Osmosis Water Treatment Plants in the Endemic Areas of Chronic Kidney Disease of Unknown Etiology (CKDu) in Sri Lanka. *Science of the Total Environment* 2020, *745*, doi:10.1016/j.scitotenv.2020.140716.
9. Dar, F.A.; Kurella, S. Recent Advances in Adsorption Techniques for Fluoride Removal – An Overview. *Groundw Sustain Dev* 2023, *23*.
10. Jha, P.K.; Tripathi, P. Arsenic and Fluoride Contamination in Groundwater: A Review of Global Scenarios with Special Reference to India. *Groundw Sustain Dev* 2021, *13*.
11. Behbahani, M.; Moghaddam, M.R.A.; Arami, M. Techno-Economical Evaluation of Fluoride Removal by Electrocoagulation Process: Optimization through Response Surface Methodology. *Desalination* 2011, *271*, 209–218, doi:10.1016/j.desal.2010.12.033.
12. Haldar, D.; Duarah, P.; Purkait, M.K. MOFs for the Treatment of Arsenic, Fluoride and Iron Contaminated Drinking Water: A Review. *Chemosphere* 2020, *251*.
13. Gangani, N.; Joshi, V.C.; Sharma, S.; Bhattacharya, A. Fluoride Contamination in Water: Remediation Strategies through Membranes. *Groundw Sustain Dev* 2022, *17*.
14. Kabay, N.; Arar, Ö.; Samatya, S.; Yüksel, Ü.; Yüksel, M. Separation of Fluoride from Aqueous Solution by Electrodialysis: Effect of Process Parameters and Other Ionic Species. *J Hazard Mater* 2008, *153*, 107–113, doi:10.1016/j.jhazmat.2007.08.024.
15. Lakshmi, M.V.V.C.; Chandana Lakshmip, M.V. V; Karthikp, K.V.S. *Removal of Fluoride from Groundwater Using Various Technologies: A Review*; 2019; Vol. 6;.
16. El Messaoudi, N.; Franco, D.S.P.; Gubernat, S.; Georgin, J.; Şenol, Z.M.; Ciğeroğlu, Z.; Allouss, D.; El Hajam, M. Advances and Future Perspectives of Water Defluoridation by Adsorption Technology: A Review. *Environ Res* 2024, *252*.
17. Gebrewold, B.D.; Werkneh, A.A.; Kijjanapanich, P.; Rene, E.R.; Lens, P.N.L.; Annachhatre, A.P. Low Cost Materials for Fluoride Removal from Groundwater. *J Environ Manage* 2024, *370*.
18. He, J.; Yang, Y.; Wu, Z.; Xie, C.; Zhang, K.; Kong, L.; Liu, J. Review of Fluoride Removal from Water Environment by Adsorption. *J Environ Chem Eng* 2020, *8*, doi:10.1016/j.jece.2020.104516.
19. Yadav, K.K.; Gupta, N.; Kumar, V.; Khan, S.A.; Kumar, A. A Review of Emerging Adsorbents and Current Demand for Defluoridation of Water: Bright Future in Water Sustainability. *Environ Int* 2018, *111*, 80–108.
20. Manna, S.; Das, P.; Basak, P.; Sharma, A.K.; Singh, V.K.; Patel, R.K.; Pandey, J.K.; Ashokkumar, V.; Pugazhendhi, A. Separation of Pollutants from Aqueous Solution Using Nanoclay and Its Nanocomposites: A Review. *Chemosphere* 2021, *280*.
21. Bahmanzadegan, F.; Ghaemi, A. A Comprehensive Review on Novel Zeolite-Based Adsorbents for Environmental Pollutant. *Journal of Hazardous Materials Advances* 2025, *17*.
22. Luo, Q.; Wei, J.; Guo, Z.; Song, Y. Adsorption and Immobilization of Phosphorus from Water and Sediments Using a Lanthanum-Modified Natural Zeolite: Performance, Mechanism and Effect. *Sep Purif Technol* 2024, *329*, doi:10.1016/j.seppur.2023.125187.
23. Sifuna Wanyonyi, F.; Fidelis, T.T.; Louis, H.; Kyalo Mutua, G.; Orata, F.; Rhyman, L.; Ramasami, P.; Pembere, A.M.S. Simulation Guided Prediction of Zeolites for the Sorption of Selected Anions from Water: Machine Learning Predictors for Enhanced Loading. *J Mol Liq* 2022, *355*, doi:10.1016/j.molliq.2022.118913.
24. Zhao, M.; Zhou, X.; Li, J.; Li, F.; Li, X.; Yu, J.; Guo, L.; Song, G.; Xiao, C.; Zhou, F.; et al. Efficient Removal of Phosphate and Fluoride from Phosphogypsum Leachate by Lanthanum-Modified Zeolite: Synchronous Adsorption Behavior and Mechanism. *J Environ Chem Eng* 2024, *12*, doi:10.1016/j.jece.2024.113294.

25. Yang, R.; Chen, J.; Zhang, Z.; Wu, D. Performance and Mechanism of Lanthanum-Modified Zeolite as a Highly Efficient Adsorbent for Fluoride Removal from Water. *Chemosphere* 2022, *307*, doi:10.1016/j.chemosphere.2022.136063.
26. LAI, Y. qing; YANG, K.; YANG, C.; TIAN, Z. liang; GUO, W. chang; LI, J. Thermodynamics and Kinetics of Fluoride Removal from Simulated Zinc Sulfate Solution by La(III)-Modified Zeolite. *Transactions of Nonferrous Metals Society of China (English Edition)* 2018, *28*, 783–793, doi:10.1016/S1003-6326(18)64711-9.
27. Chen, J.; Chen, H.; Li, X.; He, X. Adsorption Characteristics of Chitosan Loaded Zirconium-Zeolite Composite Adsorbents for Removal of F from Water. *Lizi Jiaohuan Yu Xifu/Ion Exchange and Adsorption* 2017, *33*.
28. Chen, J.; Yang, R.; Zhang, Z.; Wu, D. Removal of Fluoride from Water Using Aluminum Hydroxide-Loaded Zeolite Synthesized from Coal Fly Ash. *J Hazard Mater* 2022.
29. Ebsa, D.G. Defluoridation of Drinking Water by Modified Natural Zeolite with Cationic Surfactant, in the Case of Ziway Town, Ethiopia. *Clean Eng Technol* 2023, *12*, doi:10.1016/j.clet.2023.100596.
30. Gao, Y.; Li, M.; Ru, Y.; Fu, J. Fluoride Removal from Water by Using Micron Zirconia/Zeolite Molecular Sieve: Characterization and Mechanism. *Groundw Sustain Dev* 2021, *13*, doi:10.1016/j.gsd.2021.100567.
31. Ma, Z.; Zhang, Q.; Weng, X.; Mang, C.; Si, L.; Guan, Z.; Cheng, L.; Ma, Z.; Weng, X. Fluoride Ion Adsorption from Wastewater Using Magnesium(II), Aluminum(III) and Titanium(IV) Modified Natural Zeolite: Kinetics, Thermodynamics, and Mechanistic Aspects of Adsorption. *Journal of Water Reuse and Desalination* 2018, *8*, 479–489, doi:10.2166/wrd.2017.037.
32. Bera, B.; Saha Chowdhury, S.; Sonawane, V.R.; De, S. High Capacity Aluminium Substituted Hydroxyapatite Incorporated Granular Wood Charcoal (Al-HApC) for Fluoride Removal from Aqueous Medium: Batch and Column Study. *Chemical Engineering Journal* 2023, *466*, doi:10.1016/j.cej.2023.143264.
33. Joe-Wong, C.; Alemán-Reyes, A.; Le, N.Q.; Salerno, K.M.; Johnson, J.K.; Xia, Z.; Nachman, D.R. Fluoride Removal by Calcite and Hydroxyapatite. *Environ Sci (Camb)* 2023, *9*, 1683–1689, doi:10.1039/d2ew00826b.
34. Rathnayake, A.; Hettithanthri, O.; Sandanayake, S.; Mahatantila, K.; Rajapaksha, A.U.; Vithanage, M. Essence of Hydroxyapatite in Defluoridation of Drinking Water: A Review. *Environmental Pollution* 2022, *311*, doi:10.1016/j.envpol.2022.119882.
35. Russo, V.; D'Angelo, A.; Salvi, C.; Paparo, R.; Fortunato, M.E.; Cepollaro, E.M.; Tarallo, O.; Trifuoggi, M.; Di Serio, M.; Tesser, R. Fluoride Adsorption on Hydroxyapatite: From Batch to Continuous Operation. *J Environ Chem Eng* 2024, *12*, doi:10.1016/j.jece.2024.111973.
36. Bakhta, S.; Sadaoui, Z.; Bouazizi, N.; Samir, B.; Cosme, J.; Allalou, O.; Le Derf, F.; Vieillard, J. Successful Removal of Fluoride from Aqueous Environment Using Al(OH)3@AC: Column Studies and Breakthrough Curve Modeling. *RSC Adv* 2024, *14*, 1–14, doi:10.1039/d3ra06697e.
37. Hu, Q.; Yang, X.; Huang, L.; Li, Y.; Hao, L.; Pei, Q.; Pei, X. A Critical Review of Breakthrough Models with Analytical Solutions in a Fixed-Bed Column. *Journal of Water Process Engineering* 2024, *59*.
38. Asrori, M.R.; Santoso, A.; Sumari, S. Proofing the Presence of Metal Oxide Impregnated into Zeolite A without Calcination: XRD and FTIR Studies. *Case Studies in Chemical and Environmental Engineering* 2024, *9*, doi:10.1016/j.cscee.2024.100676.
39. Chen, W.; Tang, H.; Li, H.; Zhao, Y.; Wang, X.; Chen, J.; Chen, Z.; Zhu, Y.; Yang, W. Efficient Defluoridation of Water by Utilizing Nanosized Ce-Fe Bimetal Oxyhydroxides Encapsulated inside Porous Polystyrene Anion Exchanger. *Chemical Engineering Journal* 2023, *461*, doi:10.1016/j.cej.2023.141820.
40. Adamu, D.B.; Tufa, L.T.; Lee, J.; Zereffa, E.; Segne, T.A.; Razali, M.H. Facile Synthesis of Bismuth and Iron Co-Doped Hydroxyapatite Nanomaterials for High-Performance Fluoride Ions Adsorption. *J Environ Chem Eng* 2023, *11*, doi:10.1016/j.jece.2023.111196.
41. Mishima, K.; Du, X.; Miyamoto, N.; Kano, N.; Imaizumi, H. Experimental and Theoretical Studies on the Adsorption Mechanisms of Uranium (VI) Ions on Chitosan. *J Funct Biomater* 2018, *9*, doi:10.3390/jfb9030049.
42. Sharma, P.K.; Ayub, S.; Tripathi, C.N. Isotherms Describing Physical Adsorption of Cr(VI) from Aqueous Solution Using Various Agricultural Wastes as Adsorbents. *Cogent Eng* 2016, *3*, doi:10.1080/23311916.2016.1186857.

 doi:10.20944/preprints202502.2203.v1



43. Nguyen, D.A.; Nguyen, V.B.; Jang, A. Integrated Adsorption Using Ultrahigh-Porosity Magnesium Oxide with Multi-Output Predictive Deep Belief Networks: A Robust Approach for Fluoride Treatment. *Chemical Engineering Journal* 2024, *484*, doi:10.1016/j.cej.2024.149586.